"Stretching" the energy landscape of oxides—Effects on electrocatalysis and diffusion

Bilge Yildiz

Elastic strain engineering offers a new route to enable high-performance catalysts, electrochemical energy conversion devices, separation membranes and memristors. By applying mechanical stress, the inherent energy landscape of reactions involved in the material can be altered. This is the so-called mechano-chemical coupling. Here we discuss how elastic strain activates reactions on metals and oxides. We also present analogies to strained polymer reactions. A rich set of investigations have been performed on strained metal surfaces over the last 15 years, and the mechanistic reasons behind strain-induced reactivity are explained by an electronic structure model. On the other hand, the potential of strain engineering of oxides for catalytic and energy applications has been largely underexplored. In oxides, mechanical stress couples to reaction and diffusion kinetics by altering the oxygen defect formation enthalpy, migration energy barrier, adsorption energy, dissociation barrier, and charge transfer barrier. A generalization of the principles for stress activated reactions from polymers to metals to oxides is offered, and the prospect of using elastic strain to tune reaction and diffusion kinetics in functional oxides is discussed.
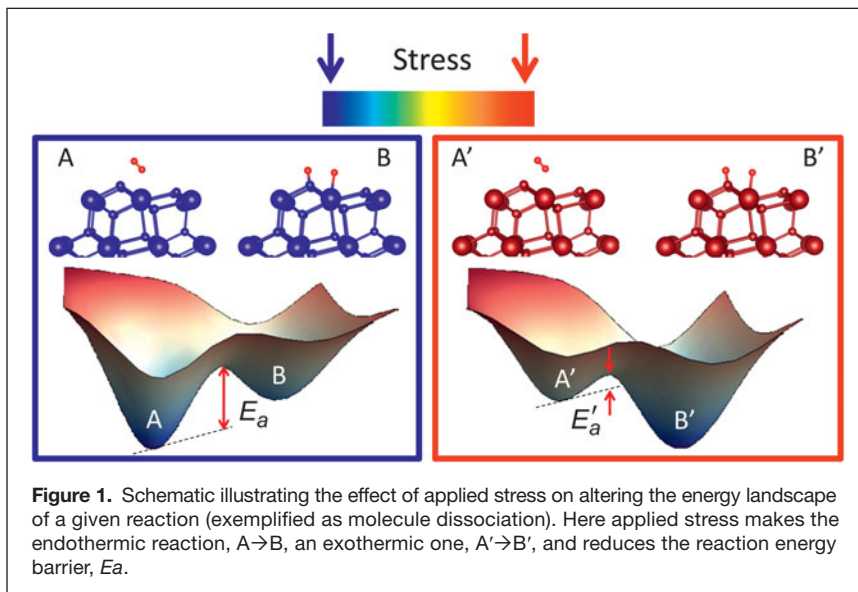
Introduction

The development of (electro)catalytic materials has traditionally relied on the design of new compositions and structures. In principle, previously unseen and desirable properties can be obtained by perturbing the structure of existing materials with elastic strain. Uncovering the fundamental mechanisms by which elastic strain alters the kinetics of (electro-)catalytic reactions can enable a new route to design highly efficient catalysts[1] and high-performance electrodes for clean energy conversion and storage devices, including fuel cells,[2–5] electrolysers,[6,7] photocatalysts,[8] and batteries.[9,10]

Elastic strain can be induced by lattice mismatch at the interface in a thin-film composite, by local applied stress, or by chemical expansion in ionic systems. The resulting stresses can direct new chemical reactions or induce unusual stress responses in materials. An influential application of elastic strain has been the activation of chemical reactions in polymers by mechanical stress at the single molecule or single bond level.[11–14] Despite the smaller elasticity of metals and oxides compared to polymers, recent work suggests that lattice strain can activate surface reactions also on metal and oxide catalysts, and anion transport in oxide membranes. In this review, we mainly discuss the fundamental effects of stress to accelerate reaction and transport kinetics in oxides, and

the potential of elastic strain engineering as a new route to improve the performance of oxide catalysts and electrocatalysts. The motivation of the work on strained oxides arises in part from the earlier seminal works on strained metal catalysts that are also reviewed here.

Lattice strain can affect chemical reactions in any material in the absence of structural transformations. A critical attribute is the stresses held in the bonds of an elastically strained material.[12,14,15] Applying internal or external stresses alters the inherent energy landscape of the system. In theory, one can turn an endothermic reaction into an exothermic one and reduce the energy barriers (**Figure 1**). This is the so-called mechano-chemical coupling, and when applied to electrochemical systems, we can introduce the term mechano-electro-chemistry. As a motivating example of this coupling, we point to a recent elegant study in polymer chemistry, relating the stress response at the molecular level to chemical reactivity. Akbulatov et al.[16,17] were able to apply forces at the spatial precision of links (bonds) between single molecules in a chain of polymeric molecules using an atomic force microscope (AFM) tip. An exponential dependence of reaction rates of cyclopropanes on the local forces were found in micrometer-long polymers and in macro-cycles. This exponential dependence demonstrates that indeed the reaction energy barriers are altered (reduced in this case) with local stresses.

Bilge Yildiz, Nuclear Science and Engineering Department, Massachusetts Institute of Technology; email byildiz@mit.edu

Figure 1. Schematic illustrating the effect of applied stress on altering the energy landscape of a given reaction (exemplified as molecule dissociation). Here applied stress makes the endothermic reaction, A→B, an exothermic one, A'→B', and reduces the reaction energy barrier, E_a.

For processes that involve the incorporation or migration of atoms, the available space in a strained lattice also contributes to changing the energy barriers, in addition to the effect of stress.
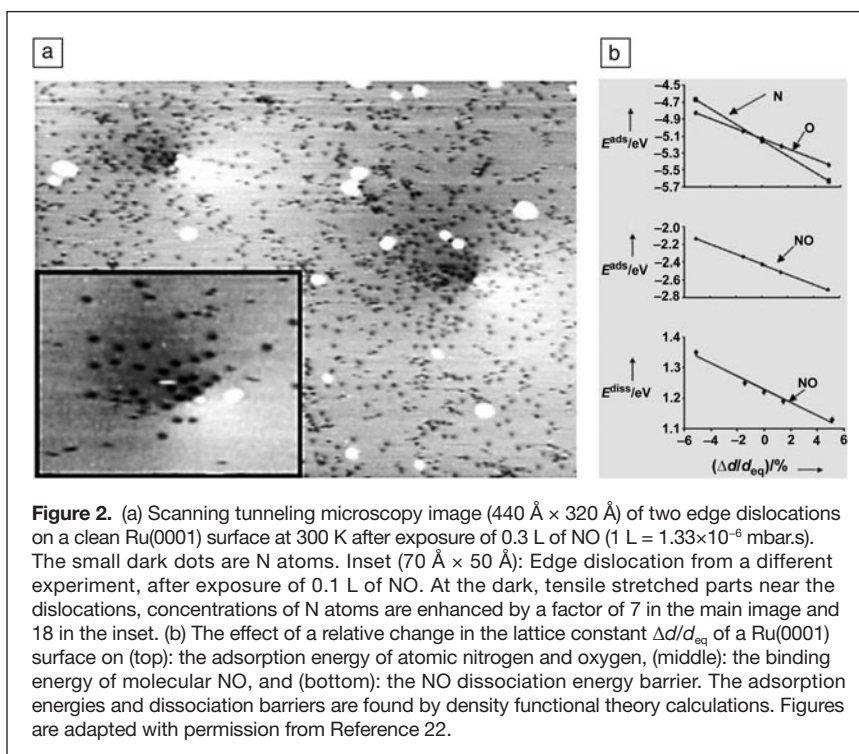
In the following, we review and discuss the effects of elastic strain on the reactivity of metal surfaces, and on the reaction and diffusion kinetics at the surface and in the bulk of ionic solids. The former is, in part, a motivator to strained oxide electrocatalysts in the latter.

Effect of strain on reactivity of metal surfaces

The body of literature in this field originates from the foundational works of Mavrikakis, Hammer, and Norskov[18] and of Gsell, Jakob, and Menzel.[19] Gsell and co-workers showed experimentally that lattice strain modified the chemisorption properties of the Ru(0001) metal surface considerably. Oxygen adsorption was found preferentially on the tensile strained zones upon local mechanical deformation of the surface by sub-surface Argon bubbles.[19] Based on this observation, Mavrikakis and co-workers used density functional theory (DFT) to assess how elastic strain changes the ability of a surface to form bonds to adsorbed atoms or molecules by altering the reaction energies and electronic structure.[18] The molecular (CO) and atomic (O) chemisorption energies as well as barriers for surface reactions (CO dissociation) were found to vary substantially on these strained lattices.[18] In both cases, the chemisorption bond was found to get stronger and the dissociation barrier to decrease as the lattice constant increased. The origin of this effect was shown to arise from the shifts in the metal d bands induced by the stress.[18,20] The

interaction between the adsorbate states and the metal d states is an important part of the reaction energy. Small changes in the environment can give rise to significant changes in the hybridization of the d states with adsorbate states.[21] When the Ru(0001) surface was expanded in a planar way parallel to the surface, d band states moved up in energy, thereby strengthening the interaction with the adsorbates in all cases. These findings led to the generalization of this effect to several catalytically important systems. This revelation had far-reaching importance for heterogeneous catalysis, because almost all catalytic reactions are preceded by bond-activated dissociation steps that are often rate limiting, and lattice strain is present in most applications involving supported catalysts due to lattice defects or by interactions with the support material.

Wintterlin et al.[22] provided the first experimental demonstration of the effect of strain field around an edge dislocation intersecting the metal surface on the local reactivity. Real catalysts are expected to have extended defects such as dislocations associated with elastic strain fields. The researchers performed scanning tunneling microscopy (STM) on Ru(0001) surfaces intersected by edge dislocations and imaged the dissociation of NO molecules. The results showed up to 18 times more enhanced reactivity to NO dissociation on the tensile strain field around the dislocation compared to that on the compressive strain field (**Figure 2**a). The calculated N, O, NO adsorption energies and the NO dissociation

Figure 2. (a) Scanning tunneling microscopy image (440 Å × 320 Å) of two edge dislocations on a clean Ru(0001) surface at 300 K after exposure of 0.3 L of NO (1 L = 1.33×10⁻⁶ mbar.s). The small dark dots are N atoms. Inset (70 Å × 50 Å): Edge dislocation from a different experiment, after exposure of 0.1 L of NO. At the dark, tensile stretched parts near the dislocations, concentrations of N atoms are enhanced by a factor of 7 in the main image and 18 in the inset. (b) The effect of a relative change in the lattice constant $\Delta d/d_{eq}$ of a Ru(0001) surface on (top): the adsorption energy of atomic nitrogen and oxygen, (middle): the binding energy of molecular NO, and (bottom): the NO dissociation energy barrier. The adsorption energies and dissociation barriers are found by density functional theory calculations. Figures are adapted with permission from Reference 22.

energy barrier were found to decrease with increasing tensile strain on Ru(0001) (Figure 2b), explaining the experimental observations by STM in the same work.

Numerous works inspired by these early results demonstrated and utilized the effect of lattice strain in other metal catalyst systems, including gold,[20,23] platinum,[15] copper,[24] nickel,[25] and dealloyed bimetallic nanoparticles.[26] By surface chemistry measurements and theoretical calculations, Strasser and co-workers provided a molecular level understanding of the unprecedented electrocatalytic activity for the electroreduction of oxygen on dealloyed fuel cell catalysts.[26] The lattice strain in the Pt shell on a Pt/Cu bimetallic core was found to be the controlling factor in the catalytic enhancement of dealloyed Pt nanoparticles. Their work experimentally demonstrated a continuous change in the oxygen $2p$ and Pt $5d$ antibonding state from above to below the Fermi level as additional compressive strain was applied, thereby weakening the adsorbate bond. This represented the first direct experimental confirmation of the computational prediction of band shifts of adsorbate-projected band structure with application of strain.

The effect of strain on metal surface reactivity is equally important for oxidation and corrosion of structural materials as it is for catalytic applications. By using a specialized scanning probe tip as an *in situ* indenter, coupled with structural and electronic characterization in the STM, Herbert et al. showed that dislocations induced by highly localized and well-defined mechanical deformation on Ni(100) exhibited enhanced reactivity toward oxidation.[27] The residual strain resulting from plastic deformation was found to locally accelerate chemical reactions of molecular oxygen. The results were also interpreted as an upshift of the d band electrons near the dislocations, measured directly by tunneling spectroscopy. The successful and widespread investigation of elastic strain on metal catalysts is owing to the presence of a well-accepted electronic structure model, namely the d band model,[21] as a reactivity descriptor.
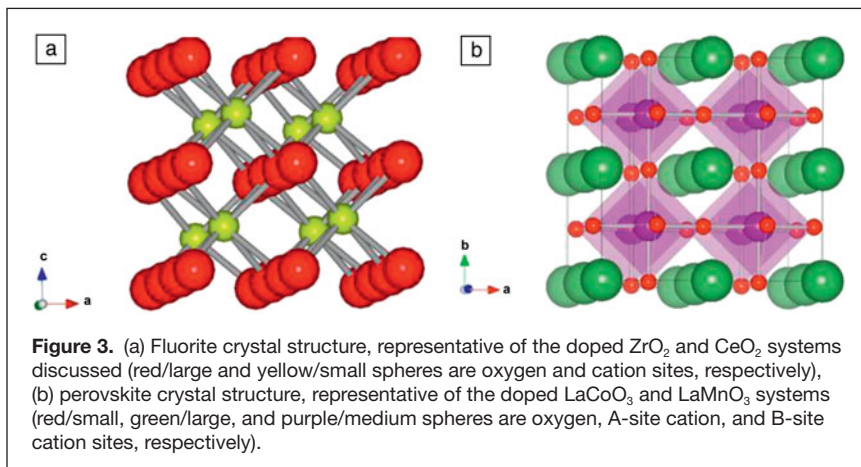
Effect of strain on ion transport and surface reactivity of oxide thin films

Discovering new oxide materials with high ionic and electronic conductivity and fast oxygen exchange kinetics on the surface is important for achieving optimal performance in a range of oxide-based electrochemical devices. To this end, an increasing number of studies have been utilizing nanoscale oxide thin films for systematic investigation of oxide interfacial properties[28,29] and for making high-density devices for energy conversion and storage with micro solid oxide fuel cells,[30,31] batteries,[32] gas conversion/reformation catalysts,[33] sensors,[34] and for information storage and processing by redox-based resistive memories.[35,36]

In nanoscale thin-film geometries, strains that originate from the lattice mismatch at interfaces can influence the properties of the material. While the coupling of strain to magnetics in multiferroic oxide heterostructures has been widely investigated (see the article by Schlom et al. in this

issue),[37–40] the coupling of lattice strain to ion conduction and surface reaction kinetics on oxide nanostructures has not been extensively explored. This topic has attracted interest rather recently in the context of oxygen transport and electrode reactions in solid oxide fuel and electrolysis cells (SOFC, SOEC).[2,54,55] Despite the small elastic strains, the stresses that can be maintained in lateral thin oxide films or vertical heterostructures are large, on the order of several GPa.[41] This suggests the presence of a noticeable mechano-chemical coupling in strained oxides for impacting the reaction and transport energy barriers and the charge-carrier density and mobility.

The surface reactivity on strained metals that we reviewed previously was broadly investigated by measuring or modeling the impact of lattice strain on the electronic structure characterized with a simple but well-established reactivity descriptor, namely the d band energy center.[21] The picture for oxide catalysts and membranes is, however, more complex. This is primarily because the metal oxides that are used are themselves chemically more complex. For example, perovskite structured compounds such as $La_{1-x}Sr_xMnO_3$ (LSM) and $La_{1-x}Sr_xCoO_3$ (LSC) serve as SOFC cathodes and separation membranes. External electromagnetic fields or mechanical strains were shown to give rise to unusual electronic and magnetic state transitions in these and other $3d$ transition metal oxides.[42,43] But the strain response of the oxygen non-stoichiometry, surface chemistry, and reactivity of these materials was not explored until recently. Perovskite oxides have two cation sublattices, dopants on each cation sublattice, and one anion sublattice, each of which can react to elastic strain. Some perovskite oxides have spin-state transitions taking place at elevated temperatures.[44] The spin state that alters internal bonding[45] is also responsive to strain via magneto-elastic coupling.[46] Furthermore, surface chemistry is not static. The composition, non-stoichiometry and structure at the surface respond to elevated temperatures by elemental segregation and phase separation,[47,48] and to oxygen chemical potential gradients and electrochemical potentials.[49] This dynamic and not well-understood behavior on perovskite oxide surfaces has made it difficult to establish universal correlation of the electronic structure to reaction kinetics, despite various attempts.[50–53] The complexity of the problem may look daunting, but recent findings on the possibility of tuning the reactivity and ion transport properties of complex oxides by "stretching" them (i.e., by elastic strain) are quite promising and worth investigating further. We first discuss the effects of strain on the ion conduction in fluorite oxides (**Figure 3**a) that serve as ion transport membranes (electrolyte) in SOFCs, SOECs, and oxygen sensors. We then extend the discussion to the effects of strain on the surface chemistry and electrocatalytic activity on more complex oxides, specifically the perovskite type oxides (Figure 3b) that serve as oxygen reduction electrocatalysts (cathode) in SOFCs,[54] oxygen evolution electrocatalysts for water splitting by electrolysis,[53] oxygen separation membranes in reactors for oxy-combustion,[55] and redox-based resistive memories.[35,36]

Figure 3. (a) Fluorite crystal structure, representative of the doped ZrO_2 and CeO_2 systems discussed (red/large and yellow/small spheres are oxygen and cation sites, respectively), (b) perovskite crystal structure, representative of the doped $LaCoO_3$ and $LaMnO_3$ systems (red/small, green/large, and purple/medium spheres are oxygen, A-site cation, and B-site cation sites, respectively).

Oxide ion conduction under lattice strain

The energy barrier for oxygen diffusion is the critical descriptor for how low a temperature the oxide electrolyte can effectively function. The most important point for us here is the potential of the lattice strain to reduce the oxygen migration energy barriers. We consider the two most widely investigated electrolyte systems for SOFCs: yttria-stabilized zirconia (YSZ) and gadolinium- or samarium-doped ceria (CGO, CSO).[54] These materials have fluorite crystal structures. They also function as oxygen sensors[56] and catalyst supports.[57–59]

Despite these being rather widely studied "old" electrolyte materials, new possibilities to identify mechano-chemically coupled ways to accelerate oxygen diffusion in them has attracted significant interest recently. The oxygen transport in these solids takes place by thermally activated migration (or hopping) of an anion from one lattice site to the nearest anion vacancy site. The energy barriers for this mechanism (1.0–1.2 eV in YSZ, 0.9–1.16 eV in CGO)[60] are too high to enable fast diffusion at intermediate temperatures (400–600°C), where the next-generation SOFCs are envisioned in contrast to the current operating temperatures of 800°C or higher. A change in the migration barrier affects the self-diffusion coefficient exponentially via the Arrhenius relation. The migration barrier depends on the separation distance and available space between the hopping sites, and the bond strength between the oxygen and the neighboring cations. The latter is affected by the local defect interactions in the context of defect association.

The search for the "fastest strain" (the strain for which conductance is

highest) in ion-conducting oxides was sparked by the report in 2008 by Garcia-Barriocanal[61] of an eight orders of magnitude increase in conductance of 1–30-nm-thick YSZ layers sandwiched between $SrTiO_3$ (STO) layers. The lattice mismatch at the interface of YSZ and STO is 7%, which is difficult to accommodate by elastic strain. To date, the exact nature of the conductance (ionic versus electronic) induced in the vicinity of the YSZ/STO interface remains debatable.[62–65] However, the community responded to this result with great curiosity over the effect of lattice strain on ion conduction.[62,66] Select works from literature in this area are summarized in **Table I**.

As can be seen in Table I, a large quantitative scatter exists in the relative improvement in ionic conductivities measured in experiments, ranging from none to 10^8 times increase. Such large scatter in experimental results has been puzzling, and may arise because of elastic stress relaxation and the presence of dislocations. Many of the experimental studies only stated the theoretical lattice mismatch between the film and the substrate or the neighboring layers, without quantifying the exact strain state in the films. It is reasonable to expect that the inconsistencies in the experimental results arise from difficulties in controlling elastic lattice

Table I. Summary of selected works from literature on the relative increase in conductivity reported for strained thin films and multilayers. The entries in the last three rows are from computational studies, and all others are experimental.

Material	Geometry	T(K)	Relative Increase in Conductivity	Ref.
YSZ/STO	Multilayer	357–531	× 10^8	61
YSZ/Y_2O_3	Multilayer	623–973	× 10	67
YSZ/STO	Multilayer	357–531	None	64
YSZ on MgO	Thin film	423–773	× 10^3	68
YSZ/STO	Multilayer	373–773	× 10^5 compared to YSZ/Al_2O_3 *Electronic conduction	63
$Ce_{0.8}Sm_{0.2}O_{2-\delta}$ (SDC)/YSZ	Multilayer	673–1073	× 10 compared to SDC × 10 compared to YSZ	69
$Ce_{0.9}Gd_{0.1}O_{2-\delta}$	Thin Film	723–1123	× 10-10^2	70
YSZ/CeO_2	Multilayer	673–973	None	71
YSZ/$Gd_2Zr_2O_7$	Multilayer	550–750	× 10^2	72
YSZ/Y_2O_3	Multilayer	793	× 2	73
$Ce_{0.9}Gd_{0.1}O_{2-\delta}$	Thin Film	673–873	× 10–0	74
YSZ on MgO	Thin Film	673–1073	× $10^{2.5}$	75
YSZ on Al_2O_3	Thin Film	673–923	× $10^{0.5}$ @ 923 K × $10^{3.5}$ @ 400 K	76
YSZ	Strained bulk	400–1000	× $10^{1.5}$ @ 1000 K, ε = 0.04 × $10^{3.5}$ @ 400 K, ε = 0.04	77
CeO_2	Strained bulk	500	× 10^4, ε = 0.04	78
ZrO_2/STO	Layered structure	0	Fluorite not stable for ε > 0.05	79

strain uniformly in the thin oxide films. Local relaxation of stress is expected to decrease or clear the effects of elastic strain on the energy landscape of the system. High-resolution strain mapping, achievable by advances in microscopy[80,81] (also see the Hÿtch and Minor article in this issue) and computation,[82] can provide one way to resolve this issue.

The results can be further complicated by the formation of dislocations upon stress relaxation, and it is also not yet clear how the dislocations alter the stability and mobility of ionic and electronic defects in their vicinity in a range of different oxides. This point is exemplified by comparing the work of Sillassen et al.[68] with that of Li et al.[72] on YSZ. Sillassen et al. claimed that the dislocations at the YSZ/MgO interface contribute to accelerating oxide ion diffusion, in addition to the impact of elastic strain. On the other hand, Li et al. claimed that dislocation-free YSZ films interfacing with $Gd_2Zr_2O_7$ layers have higher ion conductivity compared to thin YSZ films on CeO_2, which introduces misfit dislocations. More work is needed to uncover the quantitative impact of dislocations in ion conduction kinetics in oxides.

Several theoretical and computational reports dug deeper into the mechanisms by which elastic strain alone can alter the oxygen migration kinetics. These works eliminate the influence of space-charge effects, misfit dislocations, or structural changes that could be present at the interfaces of YSZ with other materials in experiments. In assessing the role of elastic strain with atomistic detail, Kushima and Yildiz combined DFT calculations of migration paths and barriers with kinetic Monte Carlo calculations of oxygen diffusivity in 9% Y_2O_3 doped YSZ.[77] They identified two competing processes that act in parallel to alter the migration barrier for oxygen. First, at low strain states, the migration barrier reduces because of the increasing migration space and the weakening of the local oxygen–cation bonds via elastic stretching. With a decrease in the migration barrier, oxygen diffusivity exhibits an exponential increase up to a critical value of tensile strain, which Kushima and Yildiz called the fastest strain.[77] This increase is more significant at lower temperatures because of the exponential effect of the migration barrier with temperature on the diffusion coefficient. The fastest strain could be viewed as the optimal elastic strain state to attain the maximum acceleration of oxygen migration kinetics. Second, at strain states higher than the fastest strain, the migration energy barrier increases and diffusivity decreases. This is because the local relaxations at large strains trap the oxygen by strengthening the local oxygen–cation bonds—the stronger the binding of oxygen, the higher the migration barrier.[83] This indicated the transition from elastic stretching

to local plastic relaxations, or may be reminiscent of structure instability at high strains.[79] The electronic charge density distribution on the cation–oxygen (C–O) bonding plane along one representative migration path in YSZ is shown in **Figure 4**a as a function of strain. For this path, elastic stretching up to 6% strain weakens the C–O bond and reduces the migration barrier of oxygen. From 6% to 8%, the breaking of a neighboring cation-oxygen re-strengthens the C–O bond and increases the migration barrier. In 9%-YSZ, the highest effective enhancement of diffusivity was predicted to occur at 4% as the fastest strain, by 3×10^1 times at 1000 K and by 7×10^3 times at 400 K (Figure 4b). The effective migration barrier is reduced by 0.4 eV.

Using a model that takes into account the isotropic pressure induced by elastic strain in YSZ, Schichtel et al.[84] estimated a 2.5 orders of magnitude increase in the ionic conductivity of YSZ at 7% strain at 573 K. Schichtel et al.'s model, however, does not take into account the relaxations of elastic strain at these large tensile strain states. Therefore, it cannot capture the plastic or structural relaxations, which may actually mitigate the diffusivity at large strains beyond elastic stretching.

De Souza and co-workers assessed the effect of strain on oxygen-vacancy migration in CeO_2 by static lattice simulations.[78] With both isotropic and biaxial strain, significant modification of the energy barriers for oxygen-vacancy migration was found. Their results also suggest that a biaxial tensile strain
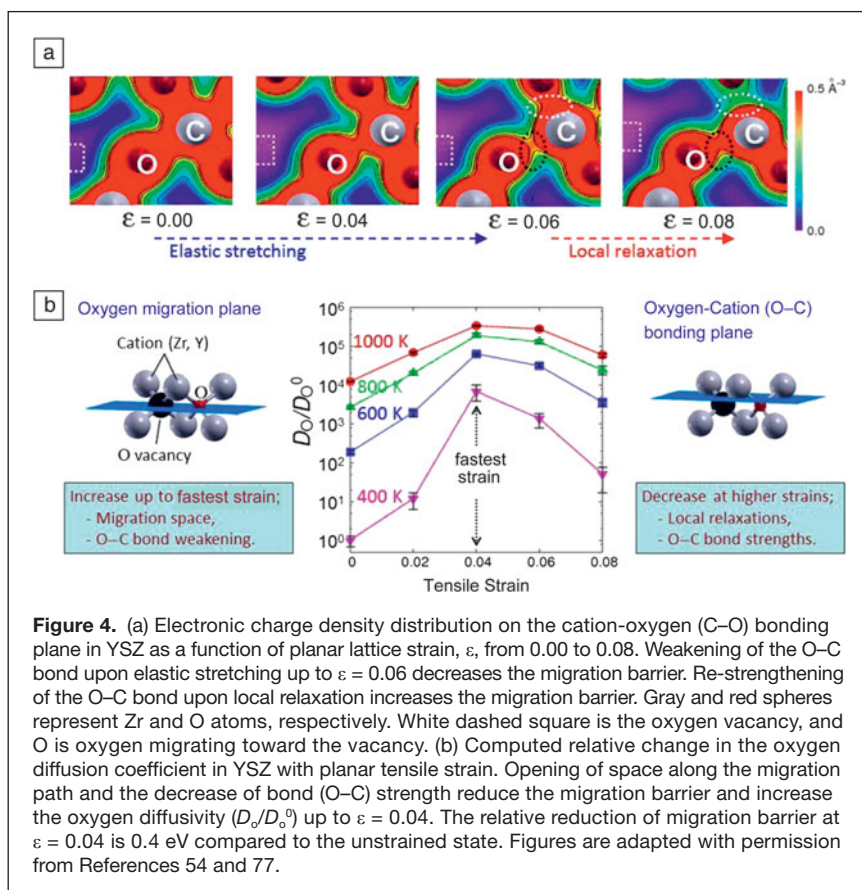
Figure 4. (a) Electronic charge density distribution on the cation-oxygen (C–O) bonding plane in YSZ as a function of planar lattice strain, ε, from 0.00 to 0.08. Weakening of the O–C bond upon elastic stretching up to ε = 0.06 decreases the migration barrier. Re-strengthening of the O–C bond upon local relaxation increases the migration barrier. Gray and red spheres represent Zr and O atoms, respectively. White dashed square is the oxygen vacancy, and O is oxygen migrating toward the vacancy. (b) Computed relative change in the oxygen diffusion coefficient in YSZ with planar tensile strain. Opening of space along the migration path and the decrease of bond (O–C) strength reduce the migration barrier and increase the oxygen diffusivity (D_o/D_o^0) up to ε = 0.04. The relative reduction of migration barrier at ε = 0.04 is 0.4 eV compared to the unstrained state. Figures are adapted with permission from References 54 and 77.

of 4% increases the in-plane conductivity at T = 500 K by close to four orders of magnitude. The predicted effect of strain on oxygen conductivity is very close to that found by Kushima and Yildiz for YSZ, suggesting that the energy landscape in these fluorite oxides, in theory, responds to strain in a similar way.

It is also interesting to note that the computational predictions of the effect of strain on ion conduction in YSZ and ceria CeO_2 are quite close to the maximum of the relative improvement in conductivity found in experiments[68] on the order of 10^3–10^4, except from the unprecedented results of Reference 61. Furthermore, the reduction in the effective activation energy for diffusion in YSZ was quantified experimentally only in two of the reported studies. Jiang et al.'s results indicated about a 0.2 eV reduction of the activation energy and Sillassen et al's experiments about 0.35 eV.[68] These are close to the reduction of effective migration barrier predicted[77] within the experimented strain ranges. Last, it is notable that none of the experimental and computational works on the effects of strain in YSZ or ceria thin films have been able to explain or replicate the conductivity values shown for the STO/YSZ/STO layered system.[61] This discrepancy suggests that strain alone cannot be responsible for the magnitude of ion conduction claimed for that particular system. Nonetheless, increases in oxide ion conductivity proposed by theory and some experiments for strained YSZ films are remarkable and are of great fundamental and practical importance. The results exemplify how local weakening of bonds in the form of elastic stretching can enable more facile oxygen migration, and thus, fast diffusion kinetics in functional oxides.

Surface chemistry and electrocatalytic activity under lattice strain

The energy landscape of surface reactions can also be altered by elastic strain, as already demonstrated on metals previously. We investigated this effect on oxides as a means to enhance their reactivity to oxygen electrocatalysis. As model electrocatalyst systems, we took the perovskite family of oxides, specifically $La_{1-x}Sr_xMnO_3$ (LSM) and $La_{1-x}Sr_xCoO_3$ (LSC), that have been the most widely studied SOFC cathode materials. These compounds also serve as ion transport membranes (ITM) in oxy-combustion[55] and have been studied widely for their magnetic properties.[46] To serve as a good cathode or ITM, they must exhibit fast oxygen reduction kinetics, or fast oxygen evolution kinetics for water splitting. While the oxygen molecule adsorption, dissociation, and charge transfer reactions are common to oxygen reduction on metals[85] and on oxides,[86] a key differentiating factor is the presence of oxygen vacancies on the latter. Both the concentration and mobility of oxygen vacancies on the surface affect oxygen reduction kinetics on oxides. The more

oxygen vacancies and the faster they move at the surface, the faster the oxygen reduction kinetics.[86] They also impact the surface electronic structure (charge transfer).[87]

How elastic strain impacts the oxygen vacancy formation in the bulk and oxygen adsorption and vacancy formation at the surface of $LaCoO_3$ (LCO) was examined by DFT calculations.[88] The effects of biaxial strain on these elementary reactions were found to manifest through two competing mechanisms that alter the strength of Co–O bonds in LCO: (1) elastic stretching of Co–O bonds, which reduces the overlap of the Co d-band and O p-band in the lattice, and (2) stress relaxations due to breaking and reforming of the Co–O bonds and due to spin state transitions. Reaction energy calculations showed each that elastic stretching facilitates each of the studied elementary processes, as long as there is an increase in the tensile stress state (**Figure 5**). This is consistent with the effect of stress on the energy landscape, as illustrated in Figure 1. The formation energy of vacancies in the bulk and on the surface of LCO decreases with increasing elastic tensile strain. A consequence of this is an increase in the concentration of oxygen vacancies as reactive sites on the surface and as diffusion-mediators in the bulk. The trend reverses when there is a stress reduction because of a strain-driven spin state transition from low- to intermediate-spin or because of plastic relaxations. Elastic stretching weakens the lattice Co–O bonds, and stress reduction strengthens the Co–O bonds and traps the lattice oxygen. Weakening of the lattice Co–O bonds at the surface allows for stronger hybridization between the d-band states of the surface Co and the 2p states of the adsorbing O_2, thereby increasing the adsorption energy of the O_2 molecule. A consequence of this is the increased coverage of adsorbed oxygen.

Reaction energies, electronic structure, spin state, and stress thresholds found in Kushima et al's work[88] suggested the possibility of tuning reactivity by strain in $LaCoO_3$ and related perovskite oxides. As a follow-up to this computational work, there have been three key experimental reports, one probing
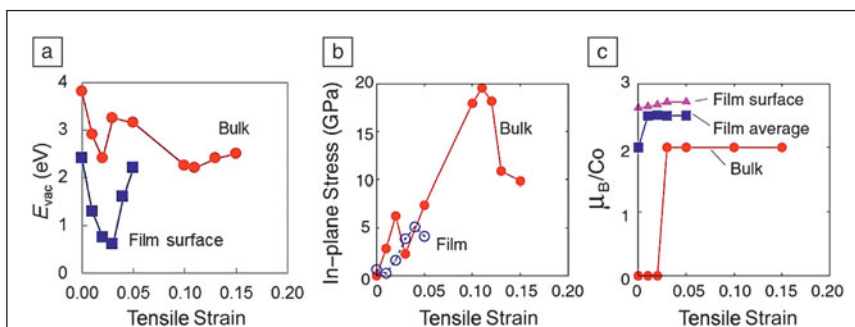
Figure 5. (a) Vacancy formation energy (E_{vac}) in the bulk and on the surface of $LaCoO_3$, (b) in-plane stress state, and (c) spin state (in μ_B/Co) as a function of planar strain in $LaCoO_3$. An increase in stress is associated with a decrease in vacancy formation enthalpies calculated by DFT. Stress relaxations due to spin state transition (at 0.03 for bulk) and due to bond breaking (at 0.1 for bulk) reverse the vacancy formation enthalpy. Figures are adapted with permission from Reference 87.

the ease of charge transfer and vacancy formation, and two quantifying the collective kinetics of oxygen exchange and diffusion as a function of strain. First, Cai et al.'s experiments[89] demonstrated that tensile strain induces a greater concentration of oxygen vacancies on $La_{0.8}Sr_{0.2}CoO_3$ (LSC) thin films (**Figure 6**c) at elevated temperatures (up to 450°C). Tensile and compressive strains were achieved by epitaxially depositing LSC thin films on single crystal $SrTiO_3$ (STO) and $LaAlO_3$ (LAO) substrates, respectively. The greater presence of oxygen vacancies on the tensile LSC film was deduced by the presence of reduced Co species in the Co 2p photoelectron spectra that was measured at elevated temperatures. This result is consistent with Kushima et al.'s predictions. Tensile strained LSC films (and also on LSM films in Reference 90) exhibited enhanced electron transfer on their surfaces at elevated temperatures above 300°C, as identified by *in situ* tunneling spectroscopy (Figure 6b). Enhancement in vacancy concentration and charge transfer on tensile strained LSC film surfaces can both accelerate oxygen reduction kinetics.

Kubicek et al. quantified the influence of lattice strain on the kinetics of oxygen exchange and diffusion on/across (100) epitaxial LSC thin films,[91] the same films as reported by Cai et al.[89] The method was based on ^{18}O isotope exchange and depth profiling with Time of Flight Secondary Ion Mass Spectroscopy (ToF-SIMS). Much faster surface exchange (~4 times) and diffusion (~10 times) were observed for the tensile strained films compared to the compressively strained films in the temperature range of 280 to 475°C (Figure 6d–e). The same outcome was found for different LSC compositions
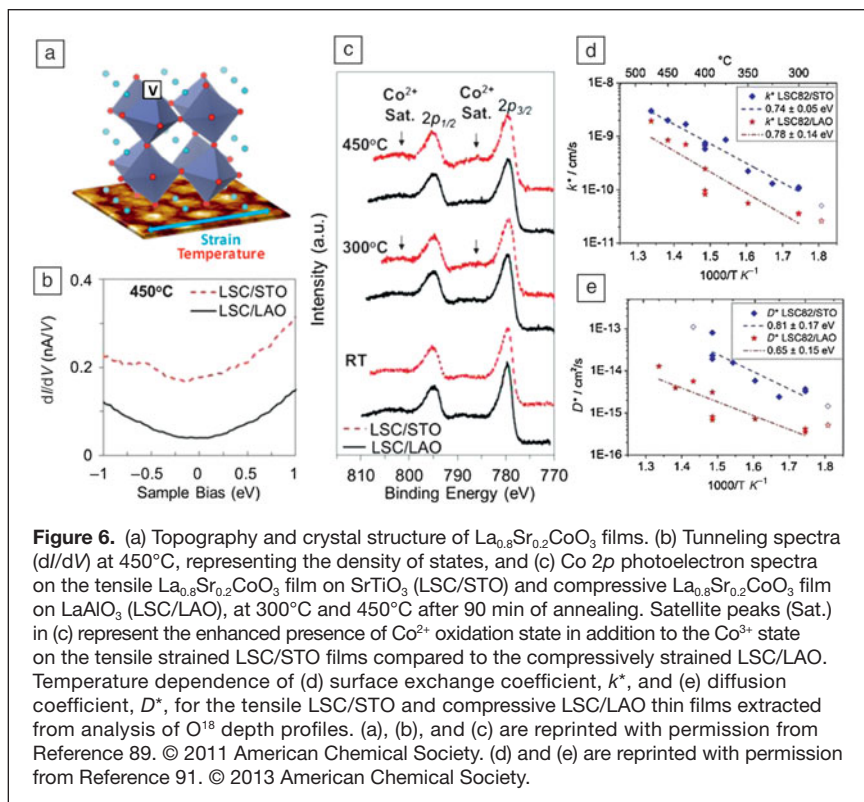
(x = 0.2 and x = 0.4) and for surface-etched films. It is not possible to deduce whether the enhancement arises from a reduction in the formation enthalpy of oxygen vacancies or an increase in the vacancy mobility or a better electron transfer activity. It is likely that all of these factors are in place.
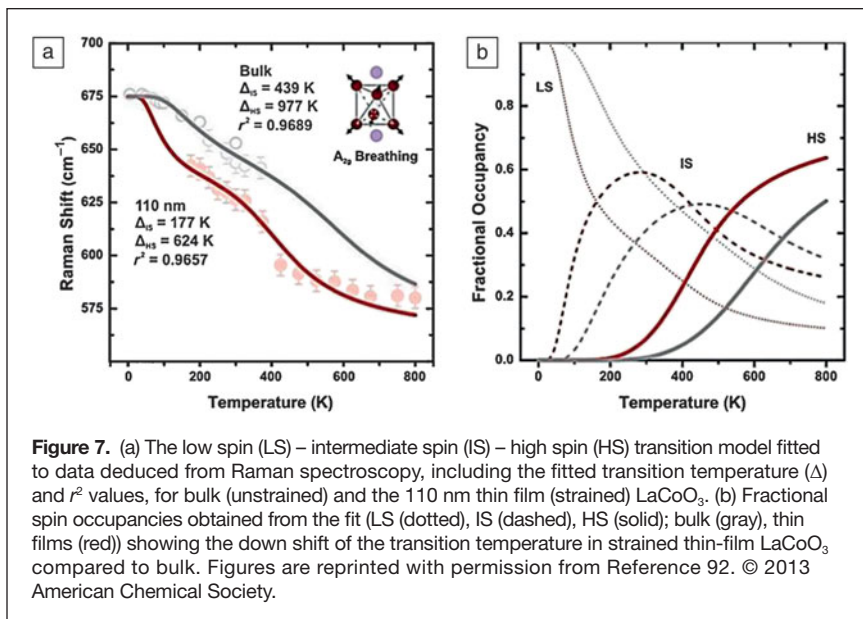
Hong et al.'s work aimed to tune the catalytic activity through strain-induced changes in the Co spin state in $LaCoO_3$ thin films.[92] They probed the Co–O bond strength by Raman spectroscopy at different temperatures to determine the relative spin occupancies of $LaCoO_3$. Strain in the LCO films reduced the spin transition temperature (**Figure 7**) and promoted the occupation of higher spin states. The spin moment increase was accompanied by the weakening of Co–O bonds. The decrease in Co–O bond strength, as suggested by Kushima et al.[88] and by Pavone et al.,[93] resulted in marked enhancements, up to two orders of magnitude, in the oxygen surface exchange kinetics detected by electrochemical impedance spectroscopy.

Generalization of stress effects on reactivity

Findings from theoretical and experimental efforts as discussed here point toward the promise of tuning oxygen surface exchange and diffusion kinetics by means of lattice strain in existing ionic and electronic conducting oxides as well as metals for catalysis and energy conversion applications. The fundamental mechanism of elastic strain driven reactions and transport is the impact of stress on the energy landscape of the system, and this is broadly valid among various classes of materials, including polymers, metals, and ceramics.[12] **Figure 8** illustrates the general trend, schematically, for several reactions and materials reviewed in this article. One can see that the more tensile the strain (within the elastic limit), the lower the vacancy formation enthalpy, vacancy migration barrier, adsorption energy (negative), and molecule dissociation energy barrier. All of this can be explained based on the weakening of the interatomic bonds in the tensile strained lattice. The concept is similar to doping materials to stress and expand the lattice, which results in lower atomic migration energy barriers.[74,94]

The trends shown in Figure 8 typically accelerate the surface reactions and bulk diffusion of oxygen at tensile strains. While this trend favors the device performance in fuel cells, electrolyzers, ion transport membranes, and even in memristors, the same effects can become detrimental in corrosion where the reactions and diffusion should be slow. For example, the predicted faster oxygen diffusion in tensile strained zirconia films implies accelerated oxidation kinetics through the passive film on zirconium alloys[95] and also faster corrosion kinetics at crack tips with tensile strain.[96]

Figure 6. (a) Topography and crystal structure of $La_{0.8}Sr_{0.2}CoO_3$ films. (b) Tunneling spectra (dI/dV) at 450°C, representing the density of states, and (c) Co 2p photoelectron spectra on the tensile $La_{0.8}Sr_{0.2}CoO_3$ film on $SrTiO_3$ (LSC/STO) and compressive $La_{0.8}Sr_{0.2}CoO_3$ film on $LaAlO_3$ (LSC/LAO), at 300°C and 450°C after 90 min of annealing. Satellite peaks (Sat.) in (c) represent the enhanced presence of Co^{2+} oxidation state in addition to the Co^{3+} state on the tensile strained LSC/STO films compared to the compressively strained LSC/LAO. Temperature dependence of (d) surface exchange coefficient, k^*, and (e) diffusion coefficient, D^*, for the tensile LSC/STO and compressive LSC/LAO thin films extracted from analysis of O^{18} depth profiles. (a), (b), and (c) are reprinted with permission from Reference 89. © 2011 American Chemical Society. (d) and (e) are reprinted with permission from Reference 91. © 2013 American Chemical Society.

Figure 7. (a) The low spin (LS) – intermediate spin (IS) – high spin (HS) transition model fitted to data deduced from Raman spectroscopy, including the fitted transition temperature (Δ) and r^2 values, for bulk (unstrained) and the 110 nm thin film (strained) $LaCoO_3$. (b) Fractional spin occupancies obtained from the fit (LS (dotted), IS (dashed), HS (solid); bulk (gray), thin films (red)) showing the down shift of the transition temperature in strained thin-film $LaCoO_3$ compared to bulk. Figures are reprinted with permission from Reference 92. © 2013 American Chemical Society.

To extend to a few more examples, we consider ceria, a technologically important catalyst, catalyst support, and ion transport membrane material. Sayle et al.'s atomistic calculations showed that the chemical reactivity of ceria nanorods to oxidize CO to CO_2 (by extracting oxygen from the surface) increased with applied tension and reduced when compressed.[97] This is still another demonstration of strain-tunable reactivity on an oxide. The same work discussed the implications and relevance of the strain-driven reactivity to a variety of important processes and applications, including TiO_2 nanoparticles for photocatalysis, mesoporous ZnS for semiconductor band-gap engineering, MgO for catalysis, and $Li-MnO_2$ lithiation-induced strain for energy storage. In another interesting and recent example, Cha et al. showed experimentally that the presence of dislocations considerably enhances the photocatalytic activity of rutile TiO_2 nanostructures.[98] The underlying reason was demonstrated to be the modification of the band-gap by the elastic strain field of dislocations.
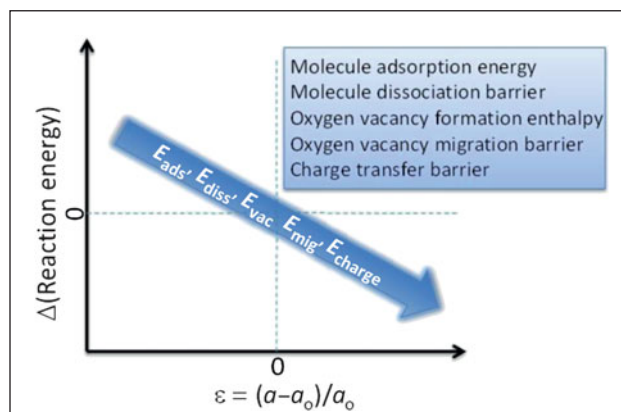
Furthermore, the fundamental mechanism here is so basic and deep that it can be generalized even to defect reactions in the bulk of a material. An extension of this understanding is to metal plasticity, which is governed by the behavior of dislocations and their interactions with point defects and defect clusters in the metal. For example, it is well known that the activation energies for the nucleation and migration (flow) of dislocations in metals depend on applied stress.[99–101] At very high strain rates, the strain localization increases the stress and decreases the energy barriers of dislocation-defect interactions.[102] These are important to account for in predicting the strength of metals over a wide range of applied strain rates and temperatures.

Conclusions and outlook

The title of this article implies that we can "stretch," that is, elastically strain functional oxides to enhance their surface reactivity and oxygen transport properties for electrochemical energy conversion applications. This theme was largely motivated by the outstanding effects of elastic strain demonstrated for reaction kinetics on metal surfaces and in polymers, as reviewed at the beginning of this article. The effect of stress on the energy landscape of the system is the key factor that couples to thermal activation and helps drive the reaction kinetics. On metals, effects of elastic strain in markedly enhancing surface reactivity are reflected as changes of the d-band electron energies. The strain-induced shifts of the d-band electron energy affect the strength of adsorption on a metal surface and the dissociation energy barriers.

For oxides, the situation is more intricate because of the chemical, electronic, and structural complexity. Despite the compounded nature of the problem, recent experimental results are encouraging, regardless of the quantitative variation among them. Based on theoretical predictions, the impact of elastic strain on reactivity and transport properties of oxides takes place via a coupling of mechanics to the energetics of elementary reactions. Specifically, oxygen defect formation enthalpy, oxygen migration energy barrier, adsorption energy, dissociation barrier, and charge transfer barrier are all altered by elastic strain. Typically, tensile strain was found to accelerate oxygen diffusion and oxygen surface exchange kinetics. The common key in different classes of materials is the stress (force) and the weakening of the interatomic bonds, which helps to activate the reactions. The reasons behind the quantitative variation among experimental results are thus far more difficult to resolve. Stress relaxations through structural changes, dislocation formation, and spin-state transitions can all reverse the effects of elastic strain in the material.

Figure 8. Schematic illustration for relative changes in reaction energies as a function of lattice strain, ε, in the elastic regime. The diagram qualitatively indicates the reduction of the molecule adsorption energies (E_{ads}), oxygen vacancy formation enthalpy (E_{vac}), molecule dissociation (E_{diss}), and atom migration (E_{mig}) energy barriers with increasing tensile strain.

One could broaden the implications of strain (stress) driven reactions from solid oxide fuel cells and electrolyzers to oxide-based photocatalysts, redox-based memristive switches, and oxidative corrosion, where the oxidation and reduction reactions at the surface/interface and diffusion of oxygen through an oxide phase determine the performance. Understanding how the oxygen defect chemistry is altered by strain can also help separate the indirect chemical effects of strain from its direct structural effects on the magnetic state transitions in magneto-elastic oxides.[43,103]

In summary, it seems promising that the surface reactivity and oxygen diffusion kinetics can be tuned by means of elastic strain in existing ionic and mixed conducting oxides. New opportunities for better understanding and control of this effect in oxides have been emerging through the synthesis of nanoscale strained thin films, multilayers, and vertical heterostructures and through the first-principles-based computational predictions. Designing new methods to quantify bond strengths locally in the solid state may help significantly in these investigations. More systematic investigations to determine precisely how elastic strain and dislocations alter reactivity in different oxide crystal classes are needed, as has been the case for metals for many years. This field is fertile ground for exciting new discoveries to enable highly efficient energy conversion devices, novel catalyst systems, and high-density and fast memory devices.

Acknowledgments

References

1. A.T. Bell, *Science* **299** (5613), 1688 (2003).
2. B.C.H. Steele, A. Heinzel, *Nature* **414** (6861), 345 (2001).
3. V.R. Stamenkovic, B. Fowler, B.S. Mun, G.F. Wang, P.N. Ross, C.A. Lucas, N.M. Markovic, *Science* **315** (5811), 493 (2007).
4. M.Z. Jacobson, W.G. Colella, D.M. Golden, *Science* **308** (5730), 1901 (2005).
5. J.L. Zhang, M.B. Vukmirovic, Y. Xu, M. Mavrikakis, R.R. Adzic, *Angew. Chem. Int. Ed. Engl.* **44** (14), 2132 (2005).
6. C. Costentin, S. Drouet, M. Robert, J.M. Saveant, *Science* **338** (6103), 90 (2012).
7. Y. Nakato, N. Takamori, H. Tsubomura, *Nature* **295** (5847), 312 (1982).
8. W.C. Chueh, C. Falter, M. Abbott, D. Scipio, P. Furler, S.M. Haile, A. Steinfeld, *Science* **330** (6012), 1797 (2010).
9. J.M. Tarascon, M. Armand, *Nature* **414** (6861), 359 (2001).
10. B. Kang, G. Ceder, *Nature* **458** (7235), 190 (2009).
11. M.M. Caruso, D.A. Davis, Q. Shen, S.A. Odom, N.R. Sottos, S.R. White, J.S. Moore, *Chem. Rev.* **109** (11), 5755 (2009).
12. C.R. Hickenboth, J.S. Moore, S.R. White, N.R. Sottos, J. Baudry, S.R. Wilson, *Nature* **446** (7134), 423 (2007).
13. J. Liang, M. Fernandez, *ACS Nano* **3** (7), 1628 (2009).
14. D.A. Davis, A. Hamilton, J.L Yang, L.D. Cremar, D. Van Gough, S.L. Potisek, M.T. Ong, P.V. Braun, T.J. Martinez, S.R. White, *Nature* **459** (7243), 68 (2009).
15. L. Grabow, Y. Xu, M. Mavrikakis, *Phys. Chem. Chem. Phys.* **8** (29), 3369 (2006).
16. S.L. Craig, *Nature* **487** (7406), 176 (2012).
17. S. Akbulatov, Y. Tian, R. Boulatov, *J. Am. Chem. Soc.* **134** (18), 7620 (2012).
18. M. Mavrikakis, B. Hammer, J.K. Norskov, *Phys. Rev. Lett.* **81** (13), 2819 (1998).
19. M. Gsell, P. Jakob, D. Menzel, *Science* **280** (5364), 717 (1998).
20. M. Mavrikakis, P. Stoltze, J.K. Norskov, *Catal. Lett.* **64** (2-4), 101 (2000).
21. B. Hammer, J.K. Norskov, *Surf. Sci.* **343**, 211 (1995).
22. J. Wintterlin, T. Zambelli, J. Trost, J. Greeley, M. Mavrikakis, *Angew. Chem. Int. Ed. Engl.* **42** (25), 2850 (2003).
23. Y. Xu, M. Mavrikakis, *J. Phys. Chem. B* **107** (35), 9298 (2003).
24. Y. Xu, M. Mavrikakis, *Surf. Sci.* **494** (2), 131 (2001).
25. J. Greeley, W.R. Krekelberg, M. Mavrikakis, *Angew. Chem. Int. Ed. Engl.* **43** (33), 4296 (2004).
26. P. Strasser, S. Koh, T. Anniyev, J. Greeley, K. More, C.F. Yu, Z.C. Liu, S. Kaya, D. Nordlund, H. Ogasawara, *Nat. Chem.* **2** (6), 454 (2010).
27. F.W. Herbert, K.J. Van Vliet, B. Yildiz, *MRS Commun.* **2** (01), 23 (2011).
28. A. Ohmoto, H.Y. Hwang, *Nature* **427** (6973), 423 (2004).
29. N. Reyren, A.D. Caviglia, L.F. Kourkoutis, G. Hammerl, C. Richter, C.W. Schneider, T. Kopp, A.-S. Ruetschi, D. Jaccard, M. Gabay, D.A. Mueller, J.-M. Triscone, J. Mannhart, *Science* **317** (5842), 1196 (2007).
30. A. Evans, A. Bieberle-Hutter, J.L.M. Rupp, L.J. Gauckler, *J. Power Sources* **194** (1), 119 (2009).
31. R. Tolke, A. Bieberle-Hutter, A. Evans, J.L.M Rupp, L.J. Gauckler, *J. Eur. Ceram. Soc.* **32** (12), 3229 (2012).
32. J. Suntivich, H.A. Gasteiger, N. Yabuuchi, H. Nakanishi, J.B. Goodenough, Y. Shao-Horn, *Nat. Chem.* **3** (8), 647 (2011).
33. S.B. Adler, J.A. Lane, B.C.H. Steele, *J. Electrochem. Soc.* **143**, 3554 (1996).
34. N. Barsan, D. Koziej, U. Weimar, *Sensor. Actuat. B-Chem.* **121** (1), 18 (2007).
35. R. Waser, M. Aono, *Nat. Mater.* **6** (11), 833 (2007).
36. R. Waser, R. Dittmann, G. Staikov, K. Szot, *Adv. Mater.* **21** (25–26), 2632 (2009).
37. J.X. Zhang, Q. He, M. Trassin, W. Luo, D. Yi, M.D. Rossell, P. Yu, L. You, C.H. Wang, C.Y. Kuo, *Phys. Rev. Lett.* **107** (14), 147602 (2011).
38. K.T. Ko, M.H. Jung, Q. He, J.H. Lee, C.S. Woo, K. Chu, J. Seidel, B.G. Jeon, Y.S. Oh, K.H. Kim et al., *Nat. Commun.* **2**, 567 (2011).
39. Q. He, Y.H. Chu, J.T. Heron, S.Y. Yang, W.I. Liang, C.Y. Kuo, H.J. Lin, P. Yu, C.W. Liang, R.J. Zeches et al., *Nat. Commun.* **2**, 225 (2011).
40. R. Ramesh, N.A. Spaldin, *Nat. Mater.* **6** (1), 21 (2007).
41. Y. Kuru, D. Marrocchelli, S.R. Bishop, D. Chen, B. Yildiz, H.L. Tuller, *J. Electrochem. Soc.* **159** (11), F799 (2012).
42. Y. Ding, D. Haskel, Y.C. Tseng, E. Kaneshita, M. van Veenendaal, J.F. Mitchell, S.V. Sinogeikin, V. Prakapenka, H.K. Mao, *Phys. Rev. Lett.* **102** (23), 237201 (2009).
43. A.D. Rata, A. Herklotz, K. Nenkov, L. Schultz, K. Dorr, *Phys. Rev. Lett.* **100** (7), 076401 (2008).
44. J.B. Goodenough, J.S. Zhou, *Chem. Mater.* **10** (10), 2980 (1998).
45. M. Haverkort, Z. Hu, J. Cezar, T. Burnus, H. Hartmann, M. Reuther, C. Zobel, T. Lorenz, A. Tanaka, N. Brookes, *Phys. Rev. Lett.* **97** (17), 247208 (2006).
46. D. Fuchs, E. Arac, C. Pinta, S. Schuppler, R. Schneider, H. v. Löhneysen, *Phys. Rev. B* **77** (1), 014434 (2008).
47. W. Lee, J.W. Han, Y. Chen, Z. Cai, B. Yildiz, *J. Am. Chem. Soc.* **135** (21), 7909 (2013).
48. M.L. Kubicek, T. Fromling, H. Hutter, J. Fleig, *J. Electrochem. Soc.* **158** (6), B727 (2011).
49. W.C. Chueh, S.M. Haile, *Annu. Rev. Chem. Biomol.* **3**, 313 (2012).
50. W. Jung, H.L. Tuller, *Adv. Energy Mater.* **1** (6), 1184 (2011).
51. N.A. Deskins, R. Rousseau, M. Dupuis, *J. Phys. Chem. C* **114**, 5891 (2010).
52. Y.-L. Lee, J. Kleis, J. Rossmeisl, Y. Shao-Horn, D. Morgan, *Energy Environ. Sci.* **4** (10), 3966 (2011).
53. J. Suntivich, K.J. May, H.A. Gasteiger, J.B. Goodenough, Y. Shao-Horn, *Science* **334** (6061), 1383 (2011).
54. A. Chroneos, B. Yildiz, A. Tarancón, D. Parfitt, J.A. Kilner, *Energy Environ. Sci.* **4** (8), 2774 (2011).
55. M.A. Habib, M. Nemitallah, R. Ben-Mansour, *Energ. Fuel.* **27** (1), 2 (2013).
56. Y. Sugawara, K. Ogawa, H. Goto, S. Oikawa, K. Akaike, N. Komura, R. Eguchi, K. Kaji, S. Gohda, Y. Kubozono, *Sensor Actuat. B-Chem.* **171**, 544 (2012).
57. R. Si, J. Raitano, N. Yi, L.H. Zhang, S.W. Chan, M. Flytzani-Stephanopoulos, *Catal. Today* **180** (1), 68 (2012).
58. Z. Zhou, S. Kooi, M. Flytzani-Stephanopoulos, H. Saltsburg, *Adv. Funct Mater.* **18** (18), 2801 (2008).
59. N. Yi, R. Si, H. Saltsburg, M. Flytzani-Stephanopoulos, *Energy Environ. Sci.* **3** (6), 831 (2010).
60. V.V. Kharton, F.M.B. Marques, A. Atkinson, *Solid State Ionics* **174** (1–4), 135 (2004).
61. J. Garcia-Barriocanal, A. Rivera-Calzada, M. Varela, Z. Sefrioui, E. Iborra, C. Leon, S.J. Pennycook, J. Santamaria, *Science* **321** (5889), 676 (2008).
62. J.A. Kilner, *Nat. Mater.* **7** (11), 838 (2008).

63. A. Cavallaro, M. Burriel, J. Roqueta, A. Apostolidis, A. Bernardi, A. Tarancon, R. Srinivasan, S.N. Cook, H.L. Fraser, J.A. Kilner, *Solid State Ionics* **181** (13–14), 592 (2010).
64. X. Guo, *Science* **324** (5926), 465 (2009).
65. R.A. De Souza, A.H.H. Ramadan, *Phys. Chem. Chem. Phys.* **15** (13), 4505 (2013).
66. J.L.M. Rupp, *Solid State Ionics* **207**, 1 (2012).
67. C. Korte, A. Peters, J. Janek, D. Hesse, N. Zakharov, *Phys. Chem. Chem. Phys.* **10** (31), 4623 (2008).
68. M. Sillassen, P. Eklund, N. Pryds, E. Johnson, U. Helmersson, J. Bottiger, *Adv. Funct. Mater.* **20** (13), 2071 (2010).
69. S. Sanna, V. Esposito, A. Tebano, S. Licoccia, E. Traversa, G. Balestrino, *Small* **6** (17), 1863 (2010).
70. K.M. Kant, V. Esposito, N. Pryds, *Appl. Phys. Lett.* **100** (3), 033105 (2012).
71. D. Pergolesi, E. Fabbri, S.N. Cook, V. Roddatis, E. Traversa, J.A. Kilner, *ACS Nano* **6** (12), 10524 (2012).
72. B. Li, J.M. Zhang, T. Kaspar, V. Shutthanandan, R.C. Ewing, J. Lian, *Phys. Chem. Chem. Phys.* **15** (4), 1296 (2013).
73. H. Aydin, C. Korte, M. Rohnke, J. Janek, *Phys. Chem. Chem. Phys.* **15** (6), 1944 (2013).
74. J. Rupp, E. Fabbri, D. Marrocchelli, J.-W. Han, D. Chen, E. Traversa, H.L. Tuller, B. Yildiz, *Adv. Funct. Mater.* (2013), doi: 10.1002/adfm.201302117.
75. I. Kosacki, C.M. Rouleau, P.F. Becher, J. Bentley, D.H. Lowndes, *Solid State Ionics* **176** (13–14), 1319 (2005).
76. J. Jiang, X. Hu, W. Shen, C. Ni, J.L. Hertz, *Appl. Phys. Lett.* **102** (14), 143901 (2013).
77. A. Kushima, B. Yildiz, *J. Mater. Chem.* **20** (23), 4809 (2010).
78. R.A. De Souza, A. Ramadan, S. Horner, *Energy Environ. Sci.* **5** (1), 5445 (2012).
79. W.L. Cheah, M.W. Finnis, *J. Mater. Sci.* **47** (4), 1631 (2012).
80. C.L. Johnson, E. Snoeck, M. Ezcurdia, B. Rodríguez-González, I. Pastoriza-Santos, L.M. Liz-Marzán, M.J. Hÿtch, *Nat. Mater.* **7** (2), 120 (2007).
81. A. Béché, J.L. Rouvière, J.P. Barnes, D. Cooper, *Ultramicroscopy* **131**, 10 (2013).
82. A. Smolyanitsky, V.K. Tewary, *Nanotechnology* **22** (8), 085703 (2011).
83. A.U. Nilekar, J. Greeley, M. Mavrikakis, *Angew. Chem. Int. Ed. Engl.* **45** (42), 7046 (2006).
84. N. Schichtel, C. Korte, D. Hesseb, J. Janeka, *Phys. Chem. Chem. Phys.* **11**, 3043 (2009).
85. Y. Xu, A.V. Ruban, M. Mavrikakis, *J. Am. Chem. Soc.* **126** (14), 4717 (2004).
86. M.M. Kuklja, E.A. Kotomin, R. Merkle, Y.A. Mastrikov, J. Maier, *Phys. Chem. Chem. Phys.* **15** (15), 5443 (2013).
87. U. Diebold, *Surf. Sci. Rep.* **48** (5–8), 53 (2003).
88. A. Kushima, S. Yip, B. Yildiz, *Phys. Rev. B* **82** (11), 115435 (2010).
89. Z. Cai, Y. Kuru, J.W. Han, Y. Chen, B. Yildiz, *J. Am. Chem. Soc.* **133** (44), 17696 (2011).
90. H. Jalili, J.W. Han, Y. Kuru, Z.H. Cai, B. Yildiz, *J. Phys. Chem Lett.* **2** (7), 801 (2011).
91. M. Kubicek, Z.H. Cai, W. Ma, B. Yildiz, H. Hutter, J. Fleig, *ACS Nano* **7** (4), 3276 (2013).
92. W.T. Hong, M. Gadre, Y.L. Lee, M.D. Biegalski, H.M. Christen, D. Morgan, Y. Shao-Horn, *J. Phys. Chem Lett.* **4** (15), 2493 (2013).
93. M. Pavone, A.M. Ritzmann, E.A. Carter, *Energy Environ. Sci.* **4** (12), 4933 (2011).
94. M. Mogensen, D. Lybye, N. Bonanos, P.V. Hendriksen, F.W. Poulsen, *Elec. Soc. S2001* (28), 15 (2002).
95. A.T. Motta, *Jom-Us* **63** (8), 63 (2011).
96. G.S. Was, D. Farkas, I.M. Robertson, *Curr. Opin. Solid. St. M.* **16** (3), 134 (2012).
97. T.X.T. Sayle, M. Cantoni, U.M. Bhatta, S.C. Parker, S.R. Hall, G. Mobus, M. Molinari, D. Reid, S. Seal, D.C. Sayle, *Chem. Mater.* **24** (10), 1811 (2012).
98. S.I. Cha, K.H. Hwang, Y.H. Kim, M.J. Yun, S.H. Seo, Y.J. Shin, J.H. Moon, D.Y. Lee, *Nanoscale* **5** (2), 753 (2013).
99. T. Zhu, J. Li, A. Samanta, A. Leach, K. Gall, *Phys. Rev. Lett.* **100** (2), 025502 (2008).
100. D. Rodney, L. Proville, *Phys. Rev. B* **79** (9), 094108 (2009).
101. Y. Fan, Y.N. Osetsky, S. Yip, B. Yildiz, *Phys. Rev. Lett.* **109** (13), 135503 (2012).
102. Y. Fan, Y. Osetsky, S. Yip, B. Yildiz, *Proc. Natl. Acad. Sci. U.S.A.* 2013, in print.
103. K. Dorr, O. Bilani-Zeneli, A. Herklotz, A.D. Rata, K. Boldyreva, J.W. Kim, M.C. Dekker, K. Nenkov, L. Schultz, M. Reibold, *Eur. Phys. J. B* **71** (3), 361 (2009). □